

Development and Validation of Artery-Vein Ratio Measurement based on Deep Learning Architectures

Maninder Singh

Electronics and Communication
Engineering Department
Motilal Nehru National Institute of
Technology Allahabad
Prayagraj, INDIA
manibiet04@gmail.com

Rajeev Gupta

Electronics and Communication
Engineering Department
Motilal Nehru National Institute of
Technology Allahabad
Prayagraj, INDIA
rajeevhg@gmail.com

Basant Kumar

Electronics and Communication
Engineering Department
Motilal Nehru National Institute of
Technology Allahabad
Prayagraj, INDIA
singhbasant@mnnit.ac.in

Deepak Agrawal

Jai Prakash Narayan Apex Trauma
Center
All India Institute of Medical Sciences
New Delhi, INDIA
drdeepak@gmail.com

Abstract—This paper presents an automated measurement of retinal artery and vein blood vessels using the state-of-the-art deep learning architectures. The measurement of the artery-vein ratio plays a vital role in predicting intracranial pressure (ICP) in traumatic patients. In the proposed method, the artery-vein and optic cup-to-disc (OCD) information are extracted from the retinal fundus imaging using deep CNN (D-CNN). The process involves the preprocessing of the retinal fundus image to highlight the vessels information and OCD more clearly. Further, the feature extraction of the vessels and OCD is performed using the base architecture of D-CNN. The extracted vessels and OCD determined the artery-vein ratio. The performance of the segmented artery-vein and OCD is evaluated and analyzed. Validation of measured artery-vein and OCD has been done by comparing these values with the ground truth values. The accuracy of the segmented artery-vein is determined to be 95.21 for the HRF dataset and the segmented optic cup and disc were found to be 94.70 and 92.36, respectively for the Drishti dataset. The extracted feature of artery-vein and OCD determines the artery-vein ratio using the connected component analysis. The algorithm-generated measured value is compared with the manually generated value by the two observer for the artery-vein ratio. The average error for the INSPIRE-AV dataset on total 40 images is found to be 0.15.

Keywords— deep CNN, trauma, artery vein, optic cup, optic disc

I. INTRODUCTION

The early detection and monitoring of trauma patients are needed to prevent brain damage and treatment can be provided for the caused injury. The injury caused required continuous brain screening for analysis and diagnosis using non-invasive techniques [1-4]. The retinal fundus imaging could lead to early detection and help the doctor better diagnose the brain injury. Currently, the retinal fundus imaging technique is used as a non-invasive method for the early diagnosis of glaucoma, diabetic retinopathy and hypertension cases [5-7]. In fundus imaging, diagnostic biomarkers such as blood vessels (artery-vein), optic cup and optic disc can be observed [8][9]. The observed markers can act as an early indicator for trauma patients depending on the abnormality caused by the brain injury. Moreover, the artery-vein ratio (AVR) can be

measured with the extracted feature of the segmented artery-vein, optic cup and optic disc. Few literatures have explored the possibility of monitoring intracranial pressure (ICP) in hypertension cases with artery-veins, optic cup and optic disc measurement using fundus imaging [10-16].

ICP monitoring is considered the key to optimizing the treatment of secondary brain injuries such as subarachnoid hemorrhage, cerebral edema, fatal myocardial infarction, intracranial hemorrhage and central nervous system infection to improve the treatment of traumatic brain injury. The measuring method of ICP can be invasive or non-invasive; the invasive procedures include an intraventricular catheter and lumbar puncture techniques, which are harmful to daily routines [17-19]. The non-invasive methods include the measurement of optic nerve sheath diameter using ultrasonography, computed tomography and magnetic resonance imaging scan. However, for daily clinical use, the promising optic nerve sheath diameter measure using ultrasonography can be effective [19][20]. Still, it has not been validated for routine clinical use and is prone to high interobserver variability levels. To date, much literature is available for ICP monitoring, but monitoring of ICP with artery-vein and OCD measurement using fundus imaging is needed. However, there is a huge gap in research to automate these biomarker's measurement and correlate it with hypertension cases.

Many reported literatures perform the segmentation of the diagnostic markers [21-23]. The automated measurement of arteries and vein is of interest due to the complex nature of the retina blood vessels. In addition, the segmentation of the optic cup and optic disc is needed for the AVR determination based on the width is necessary for correlating with the diseased retinal images considering the case of normal, diabetic retinopathy and hypertension [24][25]. In this novel proposed work, the preprocessing of the retinal fundus image is performed to extract the information by improving the contrast, followed by the segmentation algorithm based on a deep convolutional neural network. The segmentation of the artery-vein and optic cup and optic disc is performed using the pre-trained deep network.

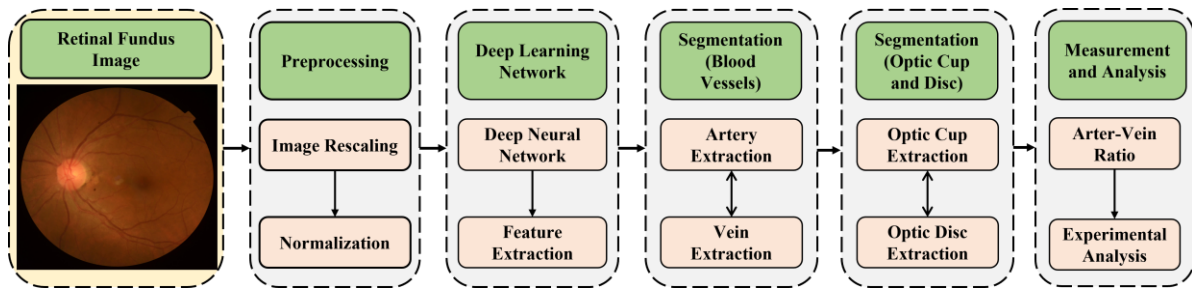


Fig. 1. Overview of the proposed approach in AVR Measurement

The segmented biomarkers are further used to determine the maximum width which is individually calculated for the artery and vein to obtain the AVR. Fig.1 depicts the overall view of the proposed approach used in AVR measurement.

The main contribution in the proposed work is summarized as follows:

1. The novel framework is designed to balance the feature map information and restructure the deep CNN model.
2. The transfer learning approach is adopted to overcome the overfitting problem with the publicly available clinically validated smaller dataset for the segmentation.
3. Validation of the segmented artery-vein and optic cup to disc using the retinal fundus is done which achieves an excellent accuracy.
4. Automatically generated artery-vein ratio is compared with the manually generated values of the two observers for the INSPIRE-AV dataset.

The rest of this paper is organized as follows: Section 2 discusses the related work contributed by researchers, followed by preprocessing steps, segmentation network and calculation of the maximum width of artery and vein. Section 3 describes the experimental work, which gives information on the dataset used for the comparison and analysis. Section 4 concludes the paper with future work and research directions.

II. PROPOSED METHOD

In the present work, a deep learning approach is used to automate the detection of the biomarker in retinal fundus imaging. It starts by performing the preprocessing steps to improve the contrast, extract the image channel and its features to segment the biomarkers. The channel extraction for the retinal fundus image in Fig. 2 is highlighted along with the histogram. The proposed work can be accomplished into three steps is explained in detail as:

Step 1: Input dataset and preprocessing:

The proposed method, first preprocessed the retinal fundus image to generalize the retinal dataset and improves the performance of the CNN architecture. These preprocessed steps will help the model to be more robust during the feature extraction stage in the deep network model. The preprocessing steps performed in various steps are explained as:

1. **Rescaling :** The dataset rescaling is performed to consider the image of the same size as it comes in different sizes during the image acquisition. Due to the different size there will be a change in the intensity of the image, therefore the image is resized to 224x224 dimensions.
2. **Normalization:** The normalization operation is performed to normalize the intensity values of an image between -1 and 1. The advantage of performing the normalized operation is during training the deep network as it will be easy to optimize the network.

Step 2: Extraction of Feature using Pretrained Network

In the field of medical imaging, acquiring large datasets is often challenging. Due to the small sample size of the dataset, the deep learning model may not perform well and sometimes causes the overfitting due to improper distribution of the dataset. It is known that deep learning models perform well on the large number of datasets, to overcome with such problem the data augmentation technique is applied and the transfer learning approach using a pre-trained model.

1. **Data augmentation:** In training the deep learning model, as the model get deeper it is difficult to train the model for the small size dataset. The problem of a small sample dataset is solved by considering the data augmentation technique. In data augmentation, during the training process, applied the random rotations within the range of -20 to +20 degrees and random magnification within the range of 90% to 110% to diversify the dataset. These transformations were applied to the images using appropriate built-in functions available in the framework, aiming to increase the diversity of the training data and improve the model's generalization.
2. **Transfer Learning:** In the proposed work, the transfer learning approach is used to fine-tune the model. The method uses the pre-trained base architecture in the encoder-decoder module, the encoder section uses EfficientNet [26] and the decoder section uses U-net [27] (pre-trained) model to extract the features in order to segment the artery-vein for the retinal fundus image. This combination allowed us to benefit from the feature extraction capabilities of EfficientNet while leveraging U-net skip connections to retain spatial information during the upsampling process. Fig. 3 depicts the schematic diagram of an encoder-decoder architecture for artery-vein segmentation.

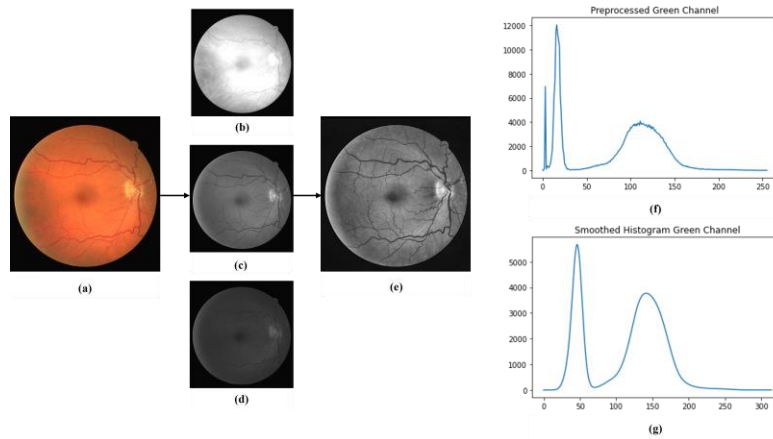


Fig. 2 Illustrates (a) Original image [29], (b) Red channel extraction, (c) Green channel extraction (d) Blue Channel extraction, (e) Normalized Green channel (f) Histogram plot of green channel extraction, and (g) Smooth histogram of the green channel.

The proposed method first inputs the preprocessed retinal fundus image which is encoded in a pre-trained model to extract the feature using the pre-trained deep neural network. The model extracts the each feature for a different layer and encodes these features as an vector. The extracted feature is then upsampled using the decoder section followed by the classification of artery and vein.

Moreover, the proposed method segments the optic cup and optic disc using the fundus imaging of the same aspect ratio considered for the artery vein. The dataset and the deep neural network work model is different. Here, the model uses the available model disc cup segmentation glaucoma network (DC – Gnet) to segment the optic cup and disc [28]. The network extracts the features for the resized image by downsampling and then upsampling the layers. The extracted features in the training phase outputs the segmented optic cup and optic disc. Further, in the training phase the filter size of 3*3 is used for the convolutional in both the segmentation. To prevent the overfitting issue dropout layer and batch normalization are added and defined the loss as binary cross-entropy. The dropout is varied for various cases and kept an 0.2 in segmentation of optic cup and disc. Overall the layers in the network uses the ReLU activation function.

Step 3: Measurement of Artery-Vein Width

The segmented optic cup and disc uses as a regions of the interest (RoI). The ROI is a circular area around the optic disc that serves as the region for artery-vein analysis. The radius of the ROI can be chosen based on a specific diameter value, such as 0.5 mm or 1 mm, which represents the desired width for the analysis. The ROI should be entirely contained within the boundaries of the segmented optic disc to ensure accurate measurements. The segmented artery vein lies within the ROI for which the maximum width of the artery and vein is obtained. The obtained artery and vein are shown in red and blue in Fig 4 (b). Using the OpenCV library, the red and blue information is separated respectively for the artery and vein and converted into grayscale. The steps follow the morphological opening operation to remove small objects or noise. Further, the connected component analysis technique is used to identify and analyze distinct objects or regions in an image. The analysis identifies individual regions or objects in the image and calculates properties such as the area, pixel indices, and pixel coordinates for each region. The process

continues repeatedly through each identified region or object in the image and examines its area. If the area is above a certain threshold (20 in this case), it further analyzes the pixels within that region to determine whether it belongs to an artery or a vein. The determination is made based on the x-coordinate of each pixel. If the x-coordinate is less than half the width of the image, it is considered part of an artery. Otherwise, it is considered part of a vein. In the process, it counts the number of arteries and veins found. The obtained retinal vessel width is determined with a computer-aided technique; the blood vessel is selected based on the segmented optic cup and optic disc information, which has a maximum diameter at a point and computing its diameter. The Euclidean distance method is used in computing its diameter in both artery and vein vessels. Moreover, the maximum width of the artery and vein is obtained and based on the clinical studies the artery vein ratio or width can be helpful, as it correlates with the ICP increases in the brain as any one of the component changes.

III. EXPERIMENTS AND RESULTS

3.1 Experiments

In this section, the experimental results have been discussed for the extraction of the artery-vein, optic cup and disc using retinal fundus imaging in the proposed work. The RITE [29], HRF [30], and LES-AV [31] publicly available datasets have been considered for artery-vein segmentation. The Drishti-GS dataset is considered for the segmentation of the optic cup and optic disc using retinal fundus imaging. Experimental operation is performed on the Google Colaboratory using the configuration of Tesla P100 PCI-E, 16GB GPU and 12.72GB RAM with the help of tensorflow and OpenCV library. The proposed work experimental setup is divided into two steps: Initially, the segmentation of the artery and vein accuracy is evaluated using the deep CNN (encoder-decoder) structure and segmentation of the optic cup and disc accuracy is evaluated using the DC-Gnet, followed by the width measurement of the artery and vein and finally correlation analysis is done. These publicly available retinal fundus images are randomly divided into a training (70%) and a validation (30%) set. Further data augmentation techniques are applied to increase the size of the dataset. For testing purposes, the publicly available database of the INSPIRE-AV [32] is considered to validate the finding of the automated AVR measurement.

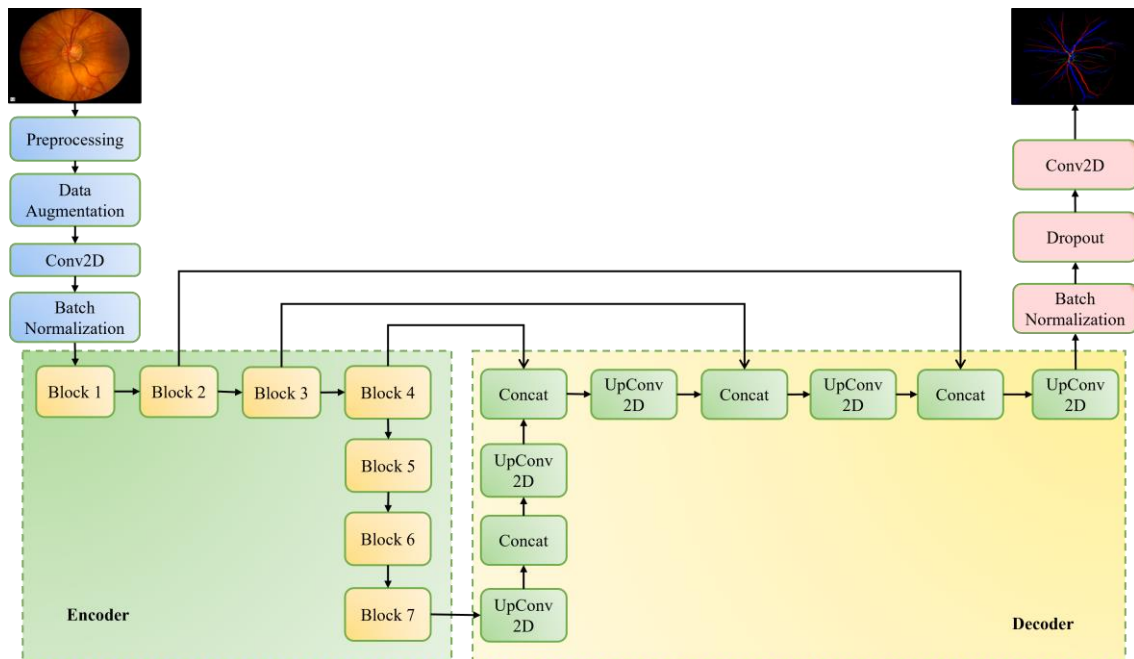


Fig. 3 depicts the schematic diagram of an encoder-decoder architecture for the segmentation of artery-vein.

3.2 Results

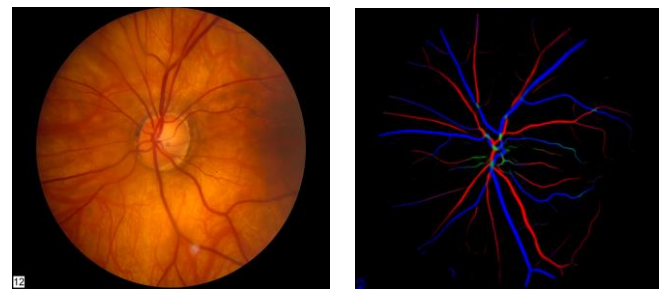
In the study, the automated measurement of artery and vein ratio has been determined. The encoder-decoder architecture is used to correctly segment the blood vessels into the artery and vein and the softmax classifier classifies the artery vein. Moreover, the segmentation of the optic cup and optic disc has been done using the DC-Gnet architecture and classify into optic cup and disc. Fig. 4 and Fig. 5 depict the extracted artery-vein and optic cup and disc, respectively. The performance of the segmented parameter has been evaluated and validated. The architecture segmented to locate the area of interest such as the artery vein and obtained the training and validation accuracy highlighted in Table 1. The performance was evaluated on three available dataset as the sensitivity and specificity of 0.91 and 0.85 respectively, for the HRF dataset were found to be satisfactory. The accuracy of the segmented artery-vein is determined to be 95.10 for the dataset.

Further, the performance of the segmented optic cup to disc was evaluated based on the dice similarity, jaccard index and accuracy. The accuracy of the segmented optic cup and disc was found to be 94.70 and 92.36. Table 2 illustrates the parameter value obtained for the segmentation of the optic cup and optic disc. Moreover, the artery-vein ratio measurement value is computed using the segmented artery vein and optic cup to disc inference graph data. The validation of the artery vein measurement was performed on the INSPIRE dataset which is publicly available. The algorithm-generated measured value was compared with the manually generated value by the two observer (Obs 1 and Obs2) for the artery-vein ratio. Table 3 illustrates the performance evaluation of the artery-vein ratio measurement. The average error for the tested dataset on total 40 images is found to be 0.15. The agreement between the measured value by the two observers and automated generated values is determined using the Bland-Altman plot. It is found that for observer 1 (Obs 1) and automated measured values, the limit lies between 0.11 to -0.08, the mean difference is 0.015, and the standard deviation of differences is 0.050. Similarly, for observer 2 (Obs 2) and

automated measured values, the limit exists for 0.10 to -0.09, the mean difference is 0.008, and the standard deviation of differences is 0.05. Fig. 6 depicts the Bland Altman plot between the observer 1 and 2 with an automated measured value of AVR. Moreover, there are certain limitations in the measurement that need to be considered in detail. The artery vein region is not considered which crosses each other and thin vessels sometimes disappear during the segmentation process in the optic cup and disc region. Another limitation in the segmentation of the optic cup and disc needs to be highlighted. With the progress of the disease in the eye the cupping generally occurs. Sometimes, this cupping leads to misjudgement of the artery-vein diagnosis, that leads to error in measurement.

TABLE 1
PERFORMANCE EVALUATION OF ARTERY-VEIN

Dataset	Training Accuracy	Validation Accuracy	Sensitivity	Specificity
RITE	92.17	91.27	0.91	0.84
HRF	95.21	93.23	0.93	0.89
LES-AV	89.11	86.87	0.88	0.91



(a) Original Image [32]

(b) Extracted Artery-Vein

Fig. 4 depicts artery-vein extracted for the INSPIRE-AV

TABLE 2
PERFORMANCE EVALUATION OF OPTIC CUP TO DISC

Parameter	Dice Similarity	Jaccard Index	Accuracy
Optic Cup	0.90	0.89	94.70
Optic Disc	0.86	0.91	92.36

TABLE 3
COMPARISON OF THE OBSERVED VALUE AND THE AUTOMATED GENERATED VALUE OF ARTERY-VEIN RATIO

Subject	Manual Measurement		Automated Measurement	Difference in Measurement	
	Obs 1	Obs 2		Obs1	Obs 2
1	0.70	0.71	0.72	0.02	0.01
2	0.63	0.68	0.67	0.04	0.01
3	0.70	0.65	0.65	0.05	0.00
4	0.65	0.64	0.65	0.00	0.01
5	0.78	0.75	0.71	0.07	0.04

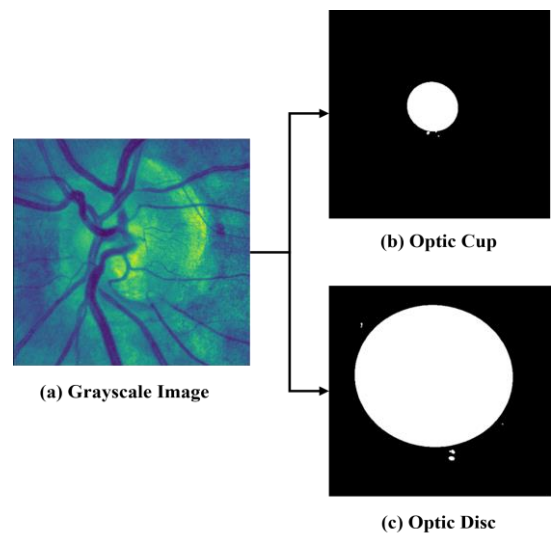


Fig. 5 Depicts (a) grayscale image of fundus, (b) optic cup and (c) disc extracted for the INSPIRE-AV

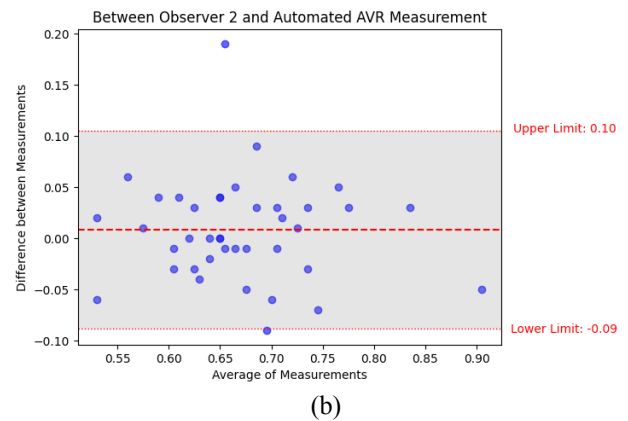
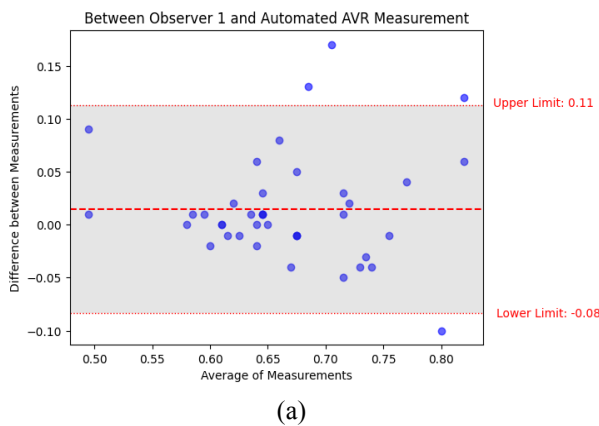


Fig. 6 Bland Altman plot depicts (a) between the observer 1 and automated measured value of AVR, (b) between the observer 2 and automated measured values of AVR.

IV. CONCLUSION

In the proposed work, an efficient method was presented for automated measurement of the artery-vein ratio using a deep learning model. The proposed work performed a segmentation of the artery-vein, optic cup and optic disc. The segmented biomarkers were used to measure the artery-vein ratio measurement. The automated measured value was validated with the help of a manually measured value on the INSPIRE dataset. In our future work, the automated measured value will be correlated with the trauma-related patients. Also, the data sample size will be expanded and at the same time more optimized model will be developed for the segmentation of biomarkers in retinal fundus imaging. Moreover, the developed algorithm will be used to develop a biomedical device which could benefit the clinician and diagnose the early symptoms of trauma injury.

REFERENCES

[1] V. V et al., "Automated detection and screening of traumatic brain injury (TBI) using computed tomography images: A comprehensive

review and future perspectives," *Int. J. Environ. Res. Public Health*, vol. 18, no. 12, p. 6499, 2021. doi:10.3390/ijerph18126499.

[2] Andersen et al., "A new novel method for assessing intracranial pressure using non-invasive fundus images: A pilot study," *Sci. Rep.*, vol. 10, no. 1, pp. 1, 2020.

[3] M. N. Khan et al., "Noninvasive monitoring intracranial pressure – A review of available modalities" *Surg. Neurol. Int.*, vol. 8, 51, 2017. doi:10.4103/sni.sni_403_16.

[4] Singh, M., Kumar, B., & Agrawal, D. (2022). Good view frames from ultrasonography (USG) video containing ONS diameter using state-of-the-art deep learning architectures. *Medical & Biological Engineering & Computing*, 60(12), 3397-3417.

[5] T. J. MacGillivray et al., "Retinal imaging as a source of biomarkers for diagnosis, characterization and prognosis of chronic illness or long-term conditions," *Br. J. Radiol.*, vol. 87, no. 1040, p. 20130832, 2014. doi:10.1259/bjr.20130832.

[6] T. Aziz et al., "Efficient and accurate hemorrhages detection in retinal fundus images using smart window features," *Appl. Sci.*, vol. 11, no. 14, p. 6391, 2021. doi:10.3390/app11146391.

[7] G. Lim et al., "Different fundus imaging modalities and technical factors in AI screening for diabetic retinopathy: A review," *Eye Vis. (Lond)*, vol. 7, pp. 21, 2020. doi:10.1186/s40662-020-00182-7.

[8] T. Li et al., "Applications of deep learning in fundus images: A review," *Med. Image Anal.*, vol. 69, p. 101971, 2021. doi:10.1016/j.media.2021.101971.

- [9] S. A. David et al., "Retinal blood vessels and optic disc segmentation using U-net," *Math. Probl. Eng.*, vol. 2022, pp. 1-11, 2022. doi:10.1155/2022/8030954.
- [10] L. D'Antona et al., "Association of intracranial pressure and spontaneous retinal venous pulsation," *JAMA Neurol.*, vol. 76, no. 12, pp. 1502-1505, 2019. doi:10.1001/jama.neuro.2019.2935.
- [11] L. Reier et al., "Optic disc edema and elevated intracranial pressure (ICP): A comprehensive review of papilledema," *Cureus*, vol. 14, no. 5, e24915, 2022. doi:10.7759/cureus.24915.
- [12] B. McCafferty et al., "The diagnostic challenge of evaluating papilledema in the pediatric patient," *Taiwan J. Ophthalmol.*, vol. 7, no. 1, p. 15-21, 2017. doi:10.4103/tjo.tjo_17_17.
- [13] Q. Zhang et al., "Association of intraocular pressure - related factors and retinal vessel diameter with optic disc rim area in subjects with and without primary open angle glaucoma," *Clin. Exp. Ophthalmol.*, vol. 46, no. 4, pp. 389-399, 2018. doi:10.1111/ceo.13042.
- [14] T. M. Dhaese et al., "Non-invasive intracranial pressure monitoring in idiopathic intracranial hypertension and lumbar puncture in pediatric patient: Case report," *Surg. Neurol. Int.*, vol. 12, 493, 2021. doi:10.25259/SNI_124_2021.
- [15] F. M. Kashif et al., "Model-based non-invasive estimation of intracranial pressure from cerebral blood flow velocity and arterial pressure," *Sci. Transl. Med.*, vol. 4, no. 129, pp. 129ra44-129ra44, 2012. doi:10.1126/scitranslmed.3003249.
- [16] E. Hamill et al., "Cup-to-disc ratio in idiopathic intracranial hypertension without papilloedema," *Neuro-Ophthalmology*, vol. 38, no. 2, pp. 69-73, 2014. doi:10.3109/01658107.2013.874452.
- [17] G. Valova et al., "Influence of interaction of cerebral fluids on ventricular deformation: A mathematical approach," *PLOS ONE*, vol. 17, no. 2, p. e0264395, 2022. doi:10.1371/journal.pone.0264395.
- [18] K. B. Digre et al., "A comparison of idiopathic intracranial hypertension with and without papilledema," *Headache J. Head Face Pain*, vol. 49, no. 2 (2009), p. 185-193.361, 2016: 122-127.
- [19] K. B. Evensen and P. K. Eide, "Measuring intracranial pressure by invasive, less invasive or non-invasive means: Limitations and avenues for improvement," *Fluids Barriers CNS*, vol. 17, no. 1, p. 34, 2020 May 6. doi:10.1186/s12987-020-00195-3. PMID:32375853. PMCID:PMC7201553.
- [20] M. Singh et al., "Good view frames from ultrasonography (USG) video containing ONS diameter using state-of-the-art deep learning architectures," *Med. Biol. Eng. Comput.*, vol. 60, no. 12, pp. 3397-3417, 2022. doi:10.1007/s11517-022-02680-3.
- [21] Khanal, A., & Estrada, R. (2020). Dynamic deep networks for retinal vessel segmentation. *Frontiers in Computer Science*, 2, 35.
- [22] Jian, M., Wu, R., Chen, H., Fu, L., & Yang, C. (2023). Dual-Branch-UNet: A Dual-Branch Convolutional Neural Network for Medical Image Segmentation. *CMES-Computer Modeling in Engineering & Sciences*, 137(1).
- [23] Tang, X., Zhong, B., Peng, J., Hao, B., & Li, J. (2020). Multi-scale channel importance sorting and spatial attention mechanism for retinal vessels segmentation. *Applied Soft Computing*, 93, 106353.
- [24] M. Niemeijer et al., "Automated measurement of the arteriolar-to-venular width ratio in digital color fundus photographs," *IEEE Trans. Med. Imaging*, vol. 30, no. 11, pp. 1941-1950, 2011 Nov.. doi:10.1109/TMI.2011.2159619. PMID:21690008.
- [25] R. García-Sierra et al., "Automated systems for calculating arteriovenous ratio in retinographies: A scoping review," *Diagnostics (Basel)*, vol. 12, no. 11, p. 2865, 2022 Nov. 18. doi:10.3390/diagnostics12112865. PMID:36428925. PMCID:PMC9689345.
- [26] Tan, M., & Le, Q. (2019, May). Efficientnet: Rethinking model scaling for convolutional neural networks. In *International conference on machine learning* (pp. 6105-6114). PMLR.
- [27] Ronneberger, O., Fischer, P., & Brox, T. (2015). U-net: Convolutional networks for biomedical image segmentation. In *Medical Image Computing and Computer-Assisted Intervention—MICCAI 2015: 18th International Conference, Munich, Germany, October 5-9, 2015, Proceedings, Part III 18* (pp. 234-241). Springer International Publishing.
- [28] M. Juneja et al, "DC-Gnet for detection of glaucoma in retinal fundus imaging," *Mach. Vis. Appl.*, vol. 31, no. 5, p. 34, 2020. doi:10.1007/s00138-020-01085-2.
- [29] Q. Hu et al., "Automated separation of binary overlapping trees in low-contrast color retinal images" in *Proc. Int. Conf. MICCAI*, 2013, pp. 436-443. doi:10.1007/978-3-642-40763-5_54.
- [30] J. Odstroicilik et al., "Retinal vessel segmentation by improved matched filtering: Evaluation on a new high-resolution fundus image database," *IET Image Process.*, vol. 7, no. 4, pp. 373-383, 2013. doi:10.1049/iet-ipr.2012.0455.
- [31] J. I. Orlando et al., "Towards a glaucoma risk index based on simulated hemodynamics from fundus images" in *Proc. Int. Conf. MICCAI*, 2018, pp. 65-73. doi:10.1007/978-3-030-00934-2_8.
- [32] B. Dashtbozorg et al., "An automatic graph-based approach for artery/vein classification in retinal images," *IEEE Trans. Image Process.*, vol. 23, no. 3, pp. 1073-1083, 2014. doi:10.1109/TIP.2013.2263809.